Dielectric characterization of multiferroic magnetoelectric double-perovskite $Y(Ni_{0.5}Mn_{0.5})O_3$ thin films

L.E. Coy[1,2,*], I. Fina[3], J. Ventura[1], L. Yate[4], E. Langenberg[1,5], M. C. Polo[1], C. Ferrater[1], M. Varela[1]

[1]*Departament Física Aplicada i Òptica, Universitat de Barcelona, Martí i Franquès 1, 08028 Barcelona, Spain.*

[2]*NanoBioMedical Centre and Department of Macromolecular Physics, Adam Mickiewicz University, Umultowska 85, 61-614 Poznan, Poland*

[3] *Institut de Ciència de Materials de Barcelona(ICMAB), CSIC, Campus de la UAB, 08193 Bellaterra, Spain.*

[4] *CIC biomaGUNE, Paseo Miramon 182, 20009, San Sebastian, Spain.*

[5]*Instituto de Ciència de Materials de Aragón (ICMA), Universidad de Zaragoza -CSIC, 50009 Zaragoza, Spain*

***Corresponding author: coyeme@amu.edu.pl**

Abstract

We report on functional properties of $Y(Ni_{0.5}Mn_{0.5})O_3$ epitaxial thin films, growth by pulsed laser deposition, observing clear features of its ferroelectric and ferromagnetic nature at cryogenic temperature. Temperature-dependent complex impedance spectroscopy (IS) characterization has shown a dielectric anomaly around the ferromagnetic Curie temperature (≈ 100 K) indicative of coupling between magnetic and electric orders.

Multiferroic materials, those showing ferroelectric and anti-/ferromagnetic order, are being deeply studied because of their possible applicability to spintronics technology and others if significant coupling between both (named magnetoelectric coupling) exist

[1–4] However, most of the single-phase multiferroic materials studied up to now are antiferromagnetic and ferroelectric, and those showing ferromagnetism (FM) instead of antiferromagnetism (AFM) are still few working below room temperature, ($BiMnO_3$ (BMO)),[5–7] and $GaFeO_3$[8] or at room temperature ε-$Fe2O_3$[9,10] or multicomponent transition metal oxides such as $Sr_3Co_2Fe_{24}O_{41}$[11], $Sr_3Co_2Ti_2Fe_8O_{19}$[12] and $[Pb(Zr_{0.53}Ti_{0.47})O_3]_{0.6}$-$[Pb(Fe_{0.5}Ta_{0.5})O_3]_{0.4}$ solid solutions[13–15] presenting the evident disadvantage of controlling the stoichiometry during the grow, or complex oxides without significant magnetoelectric coupling[16,17]**.** Thus research should focus on high temperature ferromagnetic ferroelectrics, where magnetoelectric coupling is intrinsic.

The design of double perovskite materials can overcome the mentioned challenges[18]. Tailoring the ($A_2BB^*O_6$) double perovskite formula, in such a way, that the interaction between the *B*-*B** ions would promote the FM ordering and the *R* at A-sites ions would cope with the FE ordering, typically atoms with long pair electrons, such Bi and Pb, are used in order to break the centrosymetryic nature of the lattice[19] A_2NiMnO_6 is an interesting family thanks to the encouraging results obtained in materials such as the multiferroic Bi_2NiMnO_6(BNMO)[19–25] and the ferromagnetic La_2NiMnO_6[26–34]. Remarkable enough, BNMO thin films present both ferromagnetic and ferroelectric orderings in the same crystalline phase[35], with a relatively high ferroic order temperatures (T_{FM}≈140K[20], T_{FE}≈485K). These results place double layered perovskite as interesting materials that may fulfil the mentioned functionalities, meaning having both ferroic orders related and high order temperatures.

Bulk Y_2NiMnO_6(YNMO) is a ferromagnetic (FM) below (T_{FM}) 79K with a $P2_{1/C}$ monoclinic structure. The YNMO perovskite has been synthesized and their ferromagnetic ordering reported[36,37]. Thin films of YNMO have been also obtained with discrepant structural and magnetic results[38–41], and it has been discretely referred as a

ferroelectric-ferromagnetic perovskite in some studies[42,43], although, no direct experimental confirmation of its ferroelectric nature has been yet reported in the literature[44].

In this paper, we focus on the multiferroic properties of YNMO perovskite epitaxial thin films grown by Pulsed Laser Deposition(PLD). We will investigate two set of films in order to access information along different directions: YNMO(001)/ $SrTiO_3$(001), and YNMO(111)/$SrTiO_3$(111). We will show the multiferroic nature of the material with significant ferroelectric and ferromagnetic remanences at low temperature, and signatures of coupling between magnetic and electric order by means of temperature dependent impedance spectroscopy (IS).

YNMO films with thicknesses of 60 and 40 nm where grown by PLD on conductive $Nb_{(5\%)}$:STO(001) & $Nb_{(5\%)}$:STO(111) substrates respectively, in the same deposition run, at 750°C and 0.6 mbar of O_2 pressure. Sputtered Pt (≈50 nm) top electrodes were deposited ex-situ through a shadow mask, Ø=50µm. X-ray characterisation was performed a Material Research Diffractometer (MRD-PANalytical's) using Cu Kα radiation. X-ray reflectometry was used to determine the thickness of the films

Dielectric and ferroelectric measurements have been done using the top-top electric configuration method, in which two top Pt-electrodes are contacted; therefore two YNMO capacitors connected in series through the bottom electrode are measured, equivalent to measure a single capacitor with double thickness (explained in detail in ref[45–48]). Note that using this technique; we only have access to measure dielectric permittivity (ε) and polarization (P) contributions along the out-of-plane axis of the film.

Dielectric Leakage Current Compensation (DLCC)[49] and Positive-Up-Negative-Down method (PUND)[50] techniques were used to ascertain for the ferroelectric nature of the films[46] using a high frequency I-V meter (TFAnalyser2000, aixACCT Co.). Briefly, in DLCC two I-V loops at the nominal and half of the nominal frequency are recorded, and the leakage is subtracted assuming that it is frequency independent. In PUND the current is measured while applying -++-- voltage triangular pulse sequence, switchable polarization is obtained from the integration through time normalized to the electrode area of the current resulting from the subtraction of the current measured at the second (P-pulse) from the one measured at the third (U-pulse) and the one of the fourth (N-pulse) one from the one of the fifth one (D-pulse). These measurements are described in detail in[46].

Dielectric permittivity data have been extracted by means of Impedance Spectroscopy (IS) measurements. An impedance analyser (HP4129LF, Agilent Co.) was operated with excitation voltage of 50 mV at frequencies ranging from 10 Hz to 9 MHz. Impedance data have been analysed in order to extract the intrinsic dielectric permittivity of the film, as further described in this article, following analyses described elsewhere[51,52].

Low temperature and under magnetic field measurements have been carried on a cryostat equipped with a superconducting magnet (Physical Properties Measurement System (PPMS), Quantum-Design Co.)

Figure 1 shows the presence of (*00l*) family of planes reflections for the sample grown on STO(001) (**Figure 1(a)**), and (*lll*) for the one on STO(111) (**Figure 1(b)**). It can be also observed that there is no presence of any spurious phase meaning that the films are single phase. More detailed morphological and structural characterization can be found

elsewhere[40,53], in which similar films are shown to be fully textured and epitaxial. Summarizing, the use of two different substrate orientations has allowed to obtain YNMO(001)/Nb:STO(001) and YNMO(111)/Nb:STO(111) films.

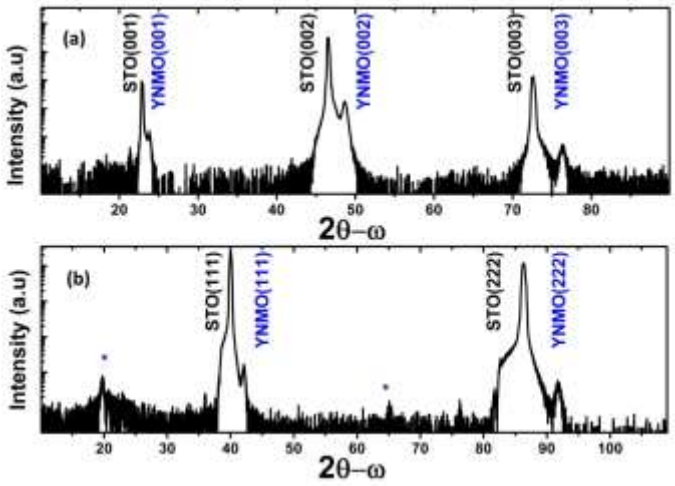

Figure 1. X-ray diffractograms of textured **(a)** YNMO(001)/STO(001), and **(b)** Pc-YNMO(111)/STO(001) films. The * shows the reflections O-YNMO(101) more details in Ref. [40]

The extracted lattice constants and unit cell volume are summarized in **Table 1**.

	a(Å)	**b(Å)**	**c(Å)**	**vol.(Å^3)**	**$\varepsilon_{[100]}$(%)**	**$\varepsilon_{[010}$(%)**	**$\varepsilon_{[001]}$(%)**
$YNMO_{BULK}$	3.69	3.92	3.74	217	-	-	-
$YNMO_{STO(001)}$	3.72	3.90	3.74	217.1	0.77	-0.54	0
$YNMO_{STO(111)}$	3.77	3.86	3.72	217	2.11	-1.62	-0.53

Table 1: Pseudocubic lattice values and strain of the YNMO(001) and YNMO(111) films, as reported in ref[40]. Unit cell volume (Vol) is calculated using the 4*(a*b*c). Film values were corrected using the substrate nominal peaks by the Nelson-Riley function.

Ferroelectric characterization has been performed in the two Pt/YNMO(001)/Nb:STO(001) and Pt/YNMO(111)/Nb:STO(111) films, having access to the properties along the c-axis for the YNMO(001) sample, and along the diagonal of the *cube* for YNMO(111) sample. In **Figure 2(a)**, current versus electric field loop measured for YNMO(001) sample at 1kHz and 5K is depicted. In that, it cannot be observed any signature of the ferroelectric current switching peaks signature of

ferroelectric behaviour. Instead only displacive current ($i_{displacive}$=1/C*dV/dt) can be observed. In **Figure 2(c)**, the polarization obtained from the integration over time of the current depicted in **Figure 2(a)**, shows clear paraelectric behaviour, evidencing the absence ferroelectric switching while applying the electric field along the c-axis. The very tinny aperture of the loop at low electric fields is ascribed only to the presence of some low leakage current (due to electronic transport across the film). Contrary, in **Figure 2(b)**, where measurement at 100Hz and 5K are shown for the YNMO(111) film, two ferroelectric switching peaks signalled with corresponding arrows, can be well appreciated. The data have been obtained after applying DLCC compensation protocol; in the inset it is shown the corresponding raw data. In both, we can observe a clear ferroelectric switching peak in the positive electric field side and a significant hysteresis in the negative electric, signalled by arrows. These data confirm the ferroelectric nature of the YNMO(111) film. In **Figure 2(d)**, the polarization versus electric field shows a polarization value around 10 $\mu C/cm^2$. The asymmetries visible in both loops (**Figure 2(b)(d)** are due to differences between the top electrodes.

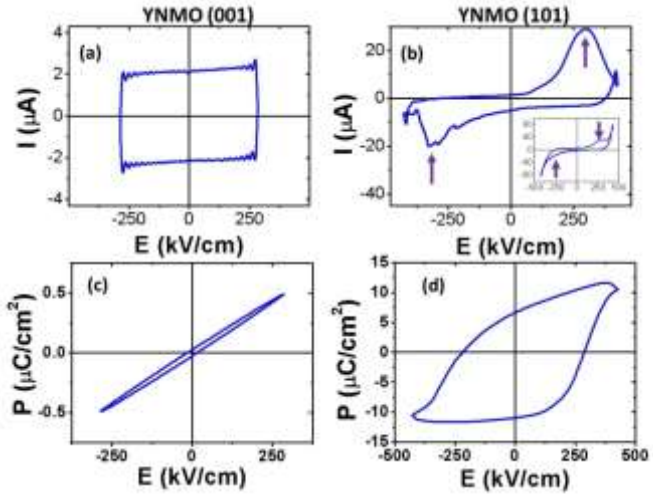

Figure 2. (a) Current versus electric field loop performed in P_C-YNMO(001) sample at 1 kHz and 5 K. (b) Current versus electric field loop performed in P_C-YNMO(111) sample at 100 Hz and 5 K. (c),(d) Polarization versus electric field loops obtained from the normalized to the area integration over time of

the current plotted in the figures (a,b) corresponding to samples P_C-YNMO(001) and P_C-YNMO(111), respectively.

Further analysis in terms of ferroelectric characterization has been performed using PUND. In **Figure 3(a)**, the current versus electric field loop measured at 10kHz and 5K after PUND subtraction is plotted. Clear ferroelectric current peaks are visible, further confirming the ferroelectric nature of the material. In **Figure 3(b)** the integrated polarization loop shows that here the remanent polarization is approximately 3.2 $\mu C/cm^2$ with a noticeable asymmetry. The discontinuity on the graph is because the different diplacive current at zero voltage during the application of P(N) and U(D) pulses.

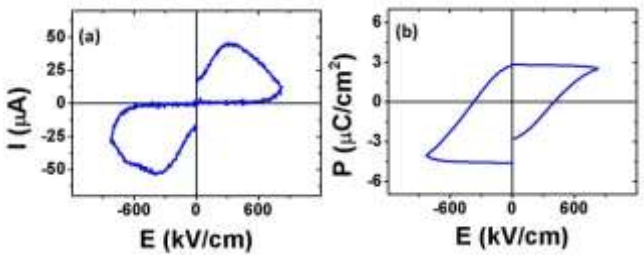

Figure 3. (a) Current versus electric field loop performed in YNMO(111) sample at 100 Hz and 5 K, after PUND subtraction. (b) Polarization versus electric field loops obtained from the normalized to the area integration over time of the current plotted in the figures (a).

Ferroelectric characterization has also been performed at higher temperatures; however, the presence of important leakage (rapidly increasing with temperature) hinders a reliable evaluation of ferroelectric polarization upon increasing temperature.

Complex impedance (-Z"vs-Z´) Nyquist representation of the measurements performed on both Pt/YNMO(001)/Nb:STO(001) and Pt/YNMO(111)/Nb:STO(111) capacitors at selected temperatures are shown in **Figure 4(a),(b)**. A double RC contribution system is clearly observed, the first semicircle dominates the higher frequencies (left-bottom side of the plot), while the second resides at lower frequencies in the spectra. The shape of

the semicircles is clear signature of two different contributions in the recorded spectrum.

Each contribution to the impedance spectra can be modelled by two circuit elements connected in parallel: one resistive, *R*, accounting for the leakage of the material, and one capacitive, *C*, accounting for the dielectric character. Additionally, we have included the non-ideal dielectric response attributed to the frequency-dependent AC conductivity of the system, *C* is commonly replaced by a constant phase element (CPE)[51,54–56] The impedance of this *R*-CPE circuit is given by

$$\mathbf{Z^*_{R\text{-}CPE}=R/(1+RQ(iw)^{\alpha})}$$

Where Q denotes the amplitude and α deals with the phase of the CPE, the typical values range from α ≤0.6- 1, being α = 1 for an ideal capacitor, and in this case C=Q. Capacitance, *C*, and dielectric permittivity, ε, values can be obtained according to the relationship $C=(Q\cdot R)^{(1/\alpha)}/R$[57], and C=εA/t, where A accounts for the area of the electrode and t for the thickness of the sample

Thus, the mentioned two contributions of the equivalent circuit have been fitted at each temperature, using the following expression:

$$\mathbf{Z^* = R_I/(1+R_I.Q_I.(iw)^{\alpha} + R_E/(1+iw.R_E.C_E)}$$

Where the first term correspond to the intrinsic($_I$) contribution of YNMO and the second term deals with the extrinsic contributions($_E$). The two RC contribution of the equivalent circuit are sketched in the insets of **Figure 4(a),(b)**, where the line through data points corresponds to the performed fitting figuring out the goodness of the fit. In the following we justify the intrinsic and extrinsic ascriptions.

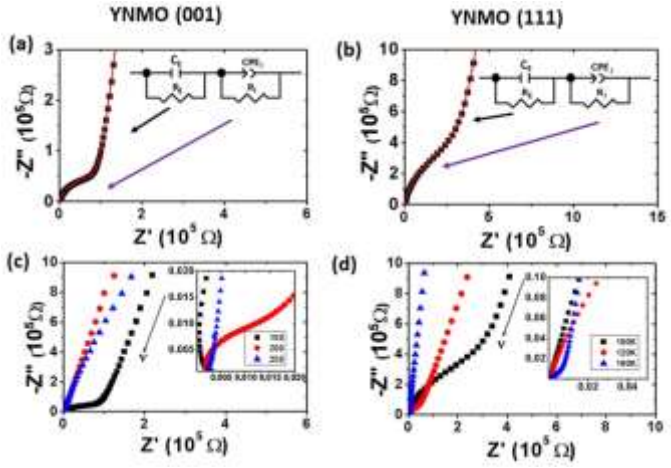

Figure 4. Selected significative plots for complex impedance (-Z"-Z´) Nqvist representation at 100K (a) and 150K(b) of YNMO(001) and YNMO(111) samples respectively, where two contributions can be clearly observed, Sketched are the fitted equivalent circuits and red lines correspond to their fitting to experimental data. (c) YNMO(001) and (d) YNMO(111) Nyquist diagrams for several temperatures. In the insets the high frequency region is zoomed.

In the low frequency contribution the extracted permittivity is as high as ≈500 for both samples, which is extremely high and differ in large amount from the already reported values denoting its extrinsic origin[37]. Therefore, it has been ascribed to interfacial extrinsic effects, as observed in other detailed studies in similar materials[51,52]. The high frequency contribution has been ascribed to the intrinsic dielectric behaviour of the film (G), and the obtained ε values (50-200) are in good agreement with the reported in the literature value for the solid solution[37]**.**

In **Figure 4(c),(d)** the Nyquist diagram for several temperatures and YNMO(001) and (111) sample, respectively, is plotted. It can be inferred from the figures that the range of temperature in which the high frequencies semicircle started to be more visible in the spectra is around 150 K for the YNMO(001) sample, and 100 K for the YNMO(111) sample. This indicates the better insulating properties of YNMO(001) sample given the decrease on the resistance of the RCPE equivalent circuit.

The temperature dependency of the extracted dielectric permittivity in both P_C-YNMO(001)/STO(001) and YNMO(111)/STO(111) is shown on **Figure 5(a),(b)**. In

YNMO(001) sample (**Figure 5(a)**) a small dielectric peak is observed at 105K. Similar feature is obtained for YNMO(111)/STO(111) film (**Figure. 5(b)**). In this case a much clear image of the dielectric anomaly is observed, showing a broad a dielectric peak at about 105K. The reliability of the results in both samples is corroborated by the low goodness-of-fit indicator $\chi 2$ which, in all temperature ranges, is $\sim 10^{-3}$, without any remarkable dispersion.

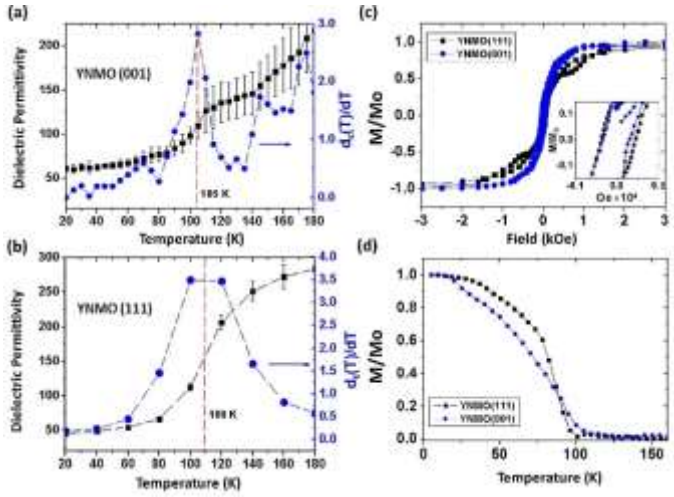

Figure 5. (a) (Left axis) plot of the dielectric permittivity of YNMO(001) and (b) YNMO(111), extracted from the complex impedance spectroscopy, as function of temperature. (Right axis) Dielectric permittivity derivative. (c) Field-Cool M(T) curve for both samples, at 1kOe. Indicated it is the transition temperature, similar in both cases. (d) M(H) measurements performed at 5K. Near zero magnetic field region is zoomed in the inset, showing the ferromagnetic nature of both samples. Magnetic field and magnetic moment have been measured along the out-of-plane direction of the film.

In **Figure 5(c)**, we show the normalized M(H)/Mo loops recorded at 5K, confirming the ferromagnetic nature of the films, which results from the ferromagnetic coupling between the adjacent nikel and manganeses ions. Mo is the saturation magnetization at 5K: for YNMO(001) and (111) films is 4.35μB/f.u. and 3.37μB/f.u., respectively It is important to remark that for B site ordered $Y_2(NiMn)O_6$, the expected magnetic moment is 5μB/f.u, however, the maximum experimental value reported to date is closer to 4.5 μB/f.u. The experimental value of our films represent a magnetization of 87% for

YNMO(001) and 67% for YNMO(111) of the theoretical bulk value. The observed magnetization reduction can be attributed to a non-ideal order of Ni-Mn ions.

In **Figure 5(d)**, it is displayed the magnetisation versus temperature dependence under a magnetic field cool of 100Oe. From the figure, it can be inferred that the Curie temperature is around 100-105K, for both films which is significantly above the 79K reported in bulk studies[36–38].

With the performed ferroelectric characterisation, we have univocally demonstrated the ferroelectric nature of YNMO. According to the results, no ferroelectric polarisation is recorded along the *c*-axis-(001), but it is along the (111) direction. Therefore, the reported results indicate that the polar axis must be contained in the *ab*-plane. These results are coherent with the theoretical work of *S. Kumar et al* [58], where it is indicated that the ferroelectric response would reside totally in the b-axis. In their work the origin of the FE ordering arose due to a re-arrangement between FM state into E*-type AFM structure, which consists of ↑-↑-↓-↓ spin chains along the in-plane cubic perovskite like (*b)* direction, with the spins chains organized in a zig-zag AFM configuration with a FM coupling in the out-of-plane direction. Is important to notice that pseudo-cubic notation has been used in our work for simplicity, the transformation used is as follows: P_C-YNMO(*001*) = o-YNMO(*001*) and P_C-YNMO(*111*)=o-YNMO(*101*)[40]. The AFM magnetic spin organization has been known to assist the ferroelecticity along the *b*-axis in perovskites materials[59,60], because the magnetic ordering breaks the spatial symmetry of the centrosymetric YNMO unit cell into a smaller enantiomorphic cell, allowing the uniaxial ferroelectric ordering. However, as already mentioned, in their work *S. Kumar et al.* YNMO was modeled as E*-type AFM[58], while in fact experimental results in this work and ~~from different groups~~ others have clearly shown a FM ordering in YNMO[38–40,43,61]. Nevertheless, their calculations showed that for a similar compound,

Sm_2NiMnO_6 a slight displacement of oxygen atoms can be induced under an external electric field, which promotes the transition from FM to E*-type AFM state, and thus the ferroelectric polarization. This predicted ferroelectric ordering would be uniaxial along the pseudo cubic *b* lattice of the Sm_2NiMnO_6 and, more importantly, could be also present in the case of the ferromagnetic YNMO (P_C-$YNMO_b$[40]) structure, because of the similarity in lattice constants between the calculated Sm_2NiMnO_6[58] and the experimental YNMO[37].

The found remanent polarization of $P_{r(111)}\approx 3$ μC/cm^2, corresponds to a projected component from the total polarization on the b-axis of 5μC/cm^2, using the as follows relation $P_{r(010)=} P_{r(111)} / \cos b/\sqrt{(a^2+b^2+c^2)}$. As a result, the polarization along the b-axis of YNMO ($P_{r(010)}$) is near the double of the predicted values, which could ascribed to the discrepancy between the lattice parameters and strain measured in our films (Table 1)and the bulk values used in the theoretical predictions, keeping in mind that the $P_{r(111)}\approx 3$ μC/cm^2 could still have leakage contribution[46]. However, It can be also argued that the observed FE response, follows a scenario closer to the one described for Sm_2NiMnO_6 in the same article, in which the applied external electric field generates a displacement on the oxygen atoms, breaking the centrosymetry of the material and thus promoting localised E*-type AFM regions in the sample. Nevertheless, such scenario would mean that the switchable area would remain under 50μm, as the electrode itself, making it very difficult to test experimentally using macromagnetic detection.

Nevertheless, the found dielectric anomaly (being signature of some electric transition) is closely positioned around the T_{FM} of the films, indicating the presence of magnetoelectric coupling more pronounced at transition temperatures[5], this suggests that the magnetic ordering is responsible for the observed dielectric peak and concomitantly the ferroelectric order found at low temperature.

In conclusion, we have experimentally proven the coexistence of both ferromagnetic and ferroelectric ordering in the YNMO perovskite, with a robust remanent polarization of $P_r \approx 3$ $\mu C/cm^2$, (and $M_r \approx 4$ μ_B comparable with the literature). The detection of a dielectric anomaly ≈100K in both samples, very close to the ferromagnetic transition, indicates some level of magnetoelectric coupling, signature of the correlation between the found ferroelectric nature of the material at low temperature and the magnetic ordering. The presented data and the theoretical predictions suggest an orientation dependent dielectric behaviour along the *b* axis of the pseudocubic YNMO unit cell. Moreover, the presence of anisotropically strained crystalline regions can be account responsible for the magnetization reduction and support the quantitative disagreement between both experiment and theory polarization values. However, it does not rule out the scenario in which E*-Type AFM could be induced by the external applied electric field, that ultimately leads to the ferroelectric ordering. Further studies are needed in order to clarify the true origin of the anisotropic ferroelectric response in YNMO.

Finally, This work demonstrates the potential interest of this manganite nickelate as multiferroic material due to the high FM and FE transition temperatures, with both ferroic orders intrinsically coupled, and paths the way to investigate other similar compounds in which the ferroelectric polarization is strongly dependent on the crystalline orientation.

Acknowledgements

The financial support by the Ministerio de Ciencia e Innovacion of the Spanish Government (grant No. BES-2009-028641 and Project Nos. MAT2011-29269-C03-03, NANOSELECT, MAT 2014-56063-C2-2-R, CSD2007-00041, MAT2015-73839-JIN and IMAGINE CSD2009-00013), and Generalitat de Catalunya (2014 SGR 734) is

acknowledged. E.C. thanks the financial support from the National Science Centre of Poland under the PRELUDIUM (UMO-2015/17/N/ST5/01988); Also the fruitful discussions and comments from Dr. Brahim Dkhil (Ecole Centrale Paris), Dr. Maciej Weisner (Adam Mickiewicz University), Dr. Sanjeev Kumar (Indian Institute of Science Education and Research) and Prof Josep Fontcuberta (ICMAB –CSIC). I.F acknowledges financial support from the Spanish Ministry of Economy and Competitiveness, through the "Severo Ochoa" Programme for Centres of Excellence in R&D (SEV- 2015-0496) also the Juan de la Cierva – Incorporación postdoctoral fellowship (IJCI-2014-19102) from the Spanish Ministry of Economy and Competitiveness of Spanish Government.

References

[1] S. a Wolf, D.D. Awschalom, R. a Buhrman, J.M. Daughton, S. von Molnár, M.L. Roukes, a Y. Chtchelkanova, and D.M. Treger, Science **294**, 1488 (2001).
[2] W. Eerenstein, N.D. Mathur, and J.F. Scott, Nature **442**, 759 (2006).
[3] C.N.R. Rao, a. Sundaresan, and R. Saha, J. Phys. Chem. Lett. **3**, 2237 (2012).
[4] A.P. Pyatakov and A.K. Zvezdin, Physics-Uspekhi **55**, 557 (2012).
[5] T. Kimura, S. Kawamoto, I. Yamada, M. Azuma, M. Takano, and Y. Tokura, Phys. Rev. B **67**, 180401 (2003).
[6] M. Gajek, M. Bibes, a. Barthélémy, K. Bouzehouane, S. Fusil, M. Varela, J. Fontcuberta, and a. Fert, Phys. Rev. B **72**, 020406 (2005).
[7] A. Sharan, J. Lettieri, Y. Jia, W. Tian, X. Pan, D.G. Schlom, and V. Gopalan, Phys. Rev. B **69**, 214109 (2004).
[8] M.K. Gupta, R. Mittal, M. Zbiri, R. Singh, S. Rols, H. Schober, and S.L. Chaplot, Phys. Rev. B **90**, 134304 (2014).
[9] M. Gich, C. Frontera, A. Roig, E. Taboada, E. Molins, H.R. Rechenberg, J.D. Ardisson, W.A.A. Macedo, C. Ritter, V. Hardy, J. Sort, V. Skumryev, and J. Nogués, Chem. Mater. **18**, 3889 (2006).
[10] M. Gich, J. Gazquez, A. Roig, A. Crespi, J. Fontcuberta, J.C. Idrobo, S.J. Pennycook, M. Varela, V. Skumryev, and M. Varela, Appl. Phys. Lett. **96**, 112508 (2010).
[11] Y. Kitagawa, Y. Hiraoka, T. Honda, T. Ishikura, H. Nakamura, and T. Kimura, Nat. Mater. **9**, 797 (2010).
[12] L. Wang, D. Wang, Q. Cao, Y. Zheng, H. Xuan, J. Gao, and Y. Du, Sci. Rep. **2**, (2012).
[13] D.M. Evans, A. Schilling, A. Kumar, D. Sanchez, N. Ortega, M. Arredondo, R.S. Katiyar, J.M. Gregg, and J.F. Scott, Nat. Commun. **4**, 1534 (2013).
[14] D.A. Sanchez, N. Ortega, A. Kumar, R. Roque-Malherbe, R. Polanco, J.F. Scott, and R.S. Katiyar, AIP Adv. **1**, 042169 (2011).
[15] J. Schiemer, M.A. Carpenter, D.M. Evans, J.M. Gregg, A. Schilling, M. Arredondo,

M. Alexe, D. Sanchez, N. Ortega, R.S. Katiyar, M. Echizen, E. Colliver, S. Dutton, and J.F. Scott, Adv. Funct. Mater. **24**, 2993 (2014).
[16] M. Trassin, N. Viart, G. Versini, J.-L. Loison, J.-P. Vola, G. Schmerber, O. Crégut, S. Barre, G. Pourroy, J.H. Lee, W. Jo, and C. Mény, Appl. Phys. Lett. **91**, 202504 (2007).
[17] K. Sharma, V. Raghavendra Reddy, A. Gupta, R.J. Choudhary, D.M. Phase, and V. Ganesan, Appl. Phys. Lett. **102**, 212401 (2013).
[18] K.F. Wang, J.-M. Liu, and Z.F. Ren, Adv. Phys. **58**, 321 (2009).
[19] S. Picozzi, K. Yamauchi, B. Sanyal, I.A. Sergienko, and E. Dagotto, Phys. Rev. Lett. **99**, 227201 (2007).
[20] M. Azuma, K. Takata, T. Saito, S. Ishiwata, Y. Shimakawa, and M. Takano, J. Am. Chem. Soc. **127**, 8889 (2005).
[21] M. Sakai, A. Masuno, D. Kan, M. Hashisaka, K. Takata, M. Azuma, M. Takano, and Y. Shimakawa, Appl. Phys. Lett. **90**, 072903 (2007).
[22] A. Ciucivara, B. Sahu, and L. Kleinman, Phys. Rev. B **76**, 064412 (2007).
[23] M. Iliev, P. Padhan, and A. Gupta, Phys. Rev. B **77**, 172303 (2008).
[24] E. Langenberg, M. Varela, M. V. García-Cuenca, C. Ferrater, M.C. Polo, I. Fina, L. Fàbrega, F. Sánchez, and J. Fontcuberta, J. Magn. Magn. Mater. **321**, 1748 (2009).
[25] E. Langenberg, J. Rebled, S. Estradé, C.J.M. Daumont, J. Ventura, L.E. Coy, M.C. Polo, M. V. García-Cuenca, C. Ferrater, B. Noheda, F. Peiró, M. Varela, and J. Fontcuberta, J. Appl. Phys. **108**, 123907 (2010).
[26] S. Kazan, F.A. Mikailzade, M. Özdemir, B. Aktaş, B. Rameev, A. Intepe, and A. Gupta, Appl. Phys. Lett. **97**, 072511 (2010).
[27] P. Padhan, P. Leclair, A. Gupta, M.A. Subramanian, and G. Srinivasan, J. Phys. Condens. Matter **21**, 306004 (2009).
[28] X. Wang, Y. Sui, Y. Li, L. Li, X. Zhang, Y. Wang, Z. Liu, W. Su, and J. Tang, Appl. Phys. Lett. **95**, 252502 (2009).
[29] M. Singh, K. Truong, S. Jandl, and P. Fournier, Phys. Rev. B **79**, 224421 (2009).
[30] M. Kitamura, I. Ohkubo, M. Kubota, Y. Matsumoto, H. Koinuma, and M. Oshima, Appl. Phys. Lett. **94**, 132506 (2009).
[31] M.N. Iliev, H. Guo, and A. Gupta, Appl. Phys. Lett. **90**, 151914 (2007).
[32] M. Hashisaka, D. Kan, A. Masuno, M. Takano, Y. Shimakawa, T. Terashima, and K. Mibu, Appl. Phys. Lett. **89**, 032504 (2006).
[33] H. Guo, J. Burgess, S. Street, A. Gupta, T.G. Calvarese, and M.A. Subramanian, Appl. Phys. Lett. **89**, 022509 (2006).
[34] N.S. Rogado, J. Li, A.W. Sleight, and M.A. Subramanian, Adv. Mater. **17**, 2225 (2005).
[35] E. Langenberg, I. Fina, P. Gemeiner, B. Dkhil, L. Fàbrega, M. Varela, and J. Fontcuberta, Appl. Phys. Lett. **100**, 022902 (2012).
[36] O. Peña, M. Bahout, Y. Ma, T. Guizouarn, D. Gutiérrez, P. Durán, and C. Moure, Mater. Sci. Eng. B **104**, 126 (2003).
[37] R.J. Booth, R. Fillman, H. Whitaker, A. Nag, R.M. Tiwari, K.V. Ramanujachary, J. Gopalakrishnan, and S.E. Lofland, Mater. Res. Bull. **44**, 1559 (2009).
[38] Y. Ma, M. Guilloux-Viry, P. Barahona, O. Peña, and C. Moure, J. Eur. Ceram. Soc. **25**, 2147 (2005).
[39] Y. Ma, M. Guilloux-Viry, P. Barahona, O. Peña, C. Moure, J. Ghilane, and P. Hapiot, Thin Solid Films **510**, 275 (2006).
[40] L.E. Coy, J. Rebled, J. Ventura, L. Yate, C. Ferrater, E. Langenberg, M.C. Polo, E. Xuriguera, F. Peiro, and M. Varela, Appl. Surf. Sci. **324**, 114 (2015).
[41] C. Xie and L. Shi, Appl. Surf. Sci. **384**, 459 (2016).
[42] J. Tang, K.W. Kemp, S. Hoogland, K.S. Jeong, H. Liu, L. Levina, M. Furukawa, X.

Wang, R. Debnath, D. Cha, K.W. Chou, A. Fischer, A. Amassian, J.B. Asbury, and E.H. Sargent, Nat. Mater. **10**, 765 (2011).
[43] R.P. Maiti, S. Dutta, M. Mukherjee, M.K. Mitra, and D. Chakravorty, J. Appl. Phys. **112**, 044311 (2012).
[44] J. Su, Z.Z. Yang, X.M. Lu, J.T. Zhang, L. Gu, C.J. Lu, Q.C. Li, J.-M. Liu, and J.S. Zhu, ACS Appl. Mater. Interfaces **7**, 13260 (2015).
[45] I. Fina, X. Martí, L. Fàbrega, F. Sànchez, and J. Fontcuberta, Thin Solid Films **518**, 4710 (2010).
[46] I. Fina, L. Fàbrega, E. Langenberg, X. Martí, F. Sánchez, M. Varela, and J. Fontcuberta, J. Appl. Phys. **109**, 074105 (2011).
[47] R. Schmidt, W. Eerenstein, T. Winiecki, F. Morrison, and P. Midgley, Phys. Rev. B **75**, 245111 (2007).
[48] R. Schmidt, J. Ventura, and E. Langenberg, Phys. Rev. B **86**, 035113 (2012).
[49] R. Meyer, R. Waser, K. Prume, T. Schmitz, and S. Tiedke, Appl. Phys. Lett. **86**, 142907 (2005).
[50] J.F. Scott, L. Kammerdiner, M. Parris, S. Traynor, V. Ottenbacher, A. Shawabkeh, and W.F. Oliver, J. Appl. Phys. **64**, 787 (1988).
[51] R. Schmidt, J. Ventura, E. Langenberg, N.M. Nemes, C. Munuera, M. Varela, M. Garcia-Hernandez, C. Leon, and J. Santamaria, Phys. Rev. B **86**, 035113 (2012).
[52] E. Langenberg, I. Fina, J. Ventura, B. Noheda, M. Varela, and J. Fontcuberta, Phys. Rev. B **86**, 085108 (2012).
[53] L.E. Coy, L. Yate, J. Ventura, K. Załęski, K. Tadyszak, C. Ferrater, M.C. Polo, and M. Varela, Appl. Surf. Sci. **387**, 864 (2016).
[54] J.R. Macdonald, Ann. Biomed. Eng. **20**, 289 (1992).
[55] P. Lunkenheimer, V. Bobnar, A. V. Pronin, A.I. Ritus, A.A. Volkov, and A. Loidl, Phys. Rev. B - Condens. Matter Mater. Phys. **66**, 521051 (2002).
[56] P. Lunkenheimer, S. Krohns, S. Riegg, S.G. Ebbinghaus, A. Reller, and A. Loidl, Eur. Phys. J. Spec. Top. **180**, 61 (2010).
[57] F. Berkemeier, M. Abouzari, and G. Schmitz, Phys. Rev. B **76**, 024205 (2007).
[58] S. Kumar, G. Giovannetti, J. van den Brink, and S. Picozzi, Phys. Rev. B **82**, 134429 (2010).
[59] T. Lottermoser, T. Lonkai, U. Amann, D. Hohlwein, J. Ihringer, and M. Fiebig, Nature **430**, 541 (2004).
[60] G. Giovannetti and J. van den Brink, Phys. Rev. Lett. **100**, 227603 (2008).
[61] M.H. Tang, Y.G. Xiao, B. Jiang, J.W. Hou, J.C. Li, and J. He, Appl. Phys. A **105**, 679 (2011).